Electronic Supplementary Information

Anti-proliferative activity of (η^6-arene)ruthenacarborane sandwich complexes against HCT116 and MCF7 cell lines

Marta Gozzi,[a] Benedikt Schwarze,[a] Menyhárt-Botond Sárosi,[a] Peter Lönnecke,[a] Dijana Drača,[b] Danijela Maksimović-Ivanić,[b] Sanja Mijatović[b] and Evamarie Hey-Hawkins*[a]

[a] *Leipzig University, Faculty of Chemistry and Mineralogy, Institute of Inorganic Chemistry, Johannisallee 29, 04103 Leipzig, Germany*

[b] *University of Belgrade, Institute of Biological Research "Siniša Stanković", Bul. Despota Stefana 142, 11060 Belgrade, Serbia*

Table of Contents

1 Characterisation of P-4 and 2

1.1 Compound P-4

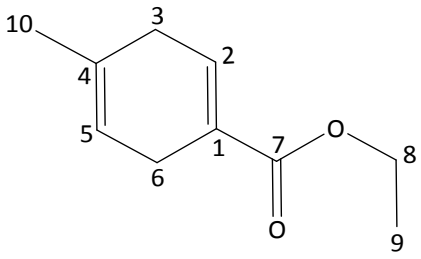

Yield: 9.62 g (49%). ^{1}H NMR (DMSO-d$_6$): δ (ppm) = 1.22 (3H, t, $^{3}J_{HH}$ = 7.1 Hz, *H*^{9}), 1.66 (3H, s, *H*^{10}), 2.71–2.86 (4H, m, *H*^{3} and *H*^{6}), 4.13 (2H, q, $^{3}J_{HH}$ = 7.2 Hz, *H*^{8}), 5.40–5.48 (1H, m, *H*^{5}), 6.84–6.90 (1H, m, *H*^{2}).

1.2 Compound 2

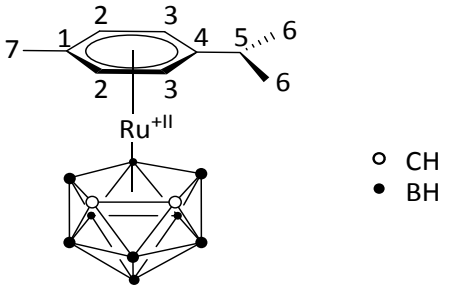

Synthesis of **2** was performed according to a modified synthesis for 3-(*p*-cym)-3,1,2-*closo*-$RuC_2B_9H_{11}$, as described in the manuscript. 0.53 g of **1** (0.98 mmol, 3.0 eq.), 0.2 g (0.33 mmol, 1.0 eq.) of **Ru2** and 20 mL of dry THF were used.

2 was obtained as pale yellow crystalline powder (R_f = 0.87 in CH_2Cl_2) in 53% yield (64 mg). Crystals of **2** suitable for X-ray diffraction analysis were obtained at 4 °C from an acetone/*n*-hexane (1:1 v/v) solution.

M.p. (from acetone/*n*-hexane): 176–178 °C. ^{1}H NMR (DMSO-d$_6$): δ (ppm) = 0.58−3.08 (9H, br, B_9H_9), 1.22 (6H, d, $^{3}J_{HH}$ = 6.9 Hz, *H*^{6}), 2.22 (3H, s, *H*^{7}), 2.80 (1H, hept, $^{3}J_{HH}$ = 6.9 Hz, *H*^{5}), 4.10 (2H, br s, $C_{cluster}H$), 6.13 (2H, d, $^{3}J_{HH}$ = 6.3 Hz, *H*^{2} or *H*^{3}), 6.20 (2H, d, $^{3}J_{HH}$ = 6.3 Hz, *H*^{2} or *H*^{3}). ^{11}B NMR (DMSO-d$_6$): δ (ppm) = −24.8 (1B, d, $^{1}J_{BH}$ = 119 Hz), −20.4 (2B, d, $^{1}J_{BH}$ = 155 Hz), −10.3 (2B, d, $^{1}J_{BH}$ = 139 Hz), −8.1 (2B, d, $^{1}J_{BH}$ = 139 Hz), −1.3 (1B, d, $^{1}J_{BH}$ = 144 Hz), 0.4 (1B, d, $^{1}J_{BH}$ = 139 Hz). ^{13}C{^{1}H} NMR (DMSO-d$_6$;): δ (ppm) = 18.7 (s, *C*^{5}), 22.8 (s, *C*^{6}), 31.4 (s, *C*^{7}), 48.1 (s, $C_{cluster}$H), 87.7 (s, *C*^{2} or *C*^{3}), 90.2 (s, *C*^{2} or *C*^{3}), 102.8 (s, *C*^{1} or *C*^{4}), 112.1 (s, *C*^{1} or *C*^{4}). IR (KBr; selected vibrations): ṽ (cm^{-1}) = 3435 (w), 3041 (w), 2963 (m), 2563 (s, ν_{BH}), 2526 (s, ν_{BH}), 1480 (m), 1377 (m), 1098 (m), 1016 (m), 986 (m), 863 (m). ESI-MS positive mode, CH_2Cl_2/MeOH): *m/z* = 391.1 (100%, [M+Na]$^{+}$). Anal. Calcd. for $C_{12}H_{25}B_9Ru$ (367.69): C, 39.20; H, 6.85. Found C, 39.03; H, 6.60.

2 Selected ^{1}H and $^{11}B\{^{1}H\}$ NMR spectra

2.1 ^{1}H NMR spectra of 2 in DMSO-d_6 and $CDCl_3$

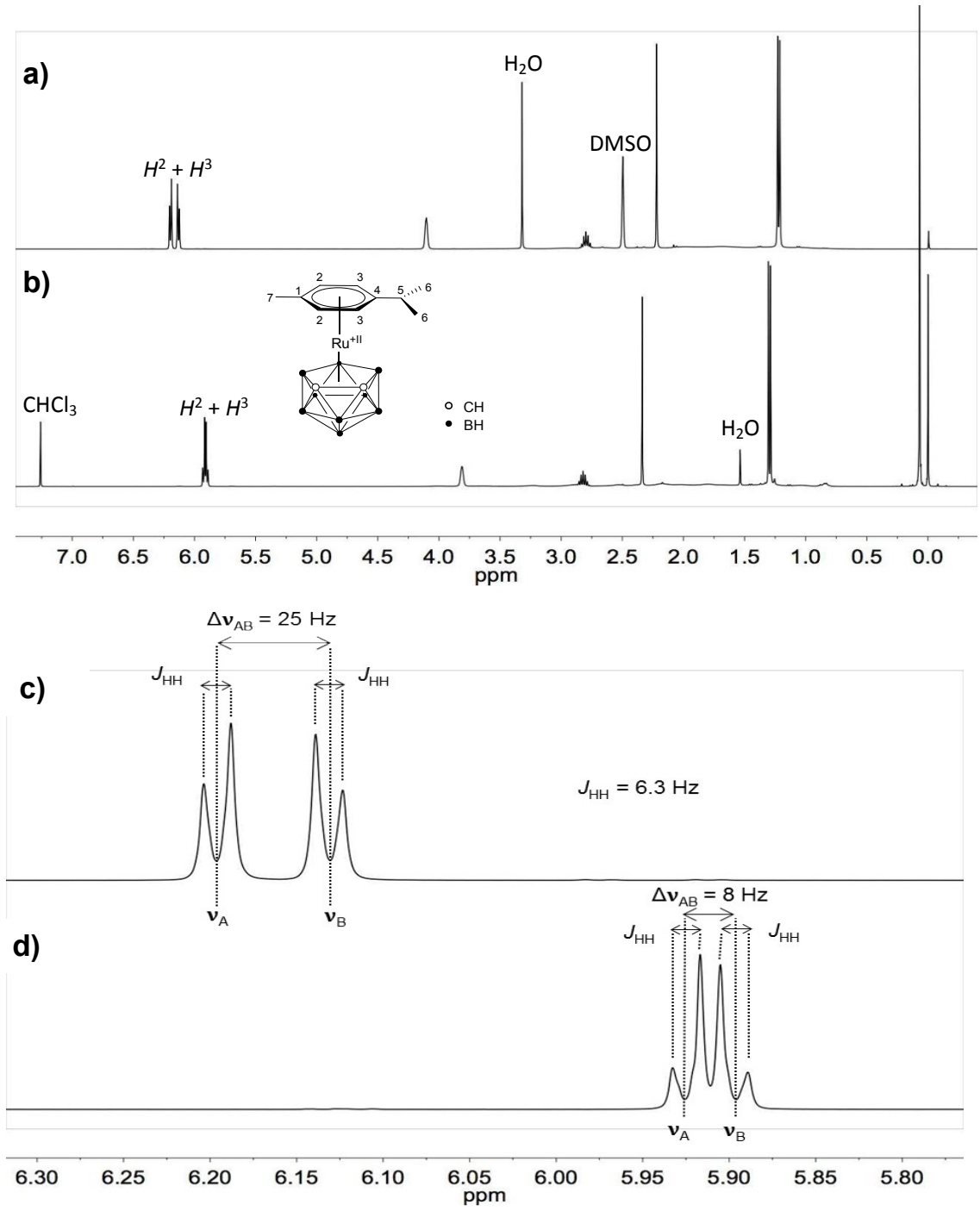

Figure S1. ^{1}H NMR spectra of **2** in DMSO-d_6 (a) and $CDCl_3$ (b). Assignment of signals for H^2 and H^3 is shown. Expanded aromatic region in DMSO-d_6 (c) and $CDCl_3$ (d) is also shown.
$\Delta\nu_{AB} = \sqrt{(\nu_1 - \nu_4)(\nu_2 - \nu_3)}$, where ν_1 is the frequency (in Hz) of the most downfield signal of the multiplet for both **c)** and **d)** traces, and ν_4 is the most upfield signal. Assignment of A and B is arbitrary.

Comparison of the ^{1}H NMR signals of **2** in $CDCl_3$ and DMSO-d_6 shows that the chemical shift of the aromatic protons is solvent-dependent (Figure S1(c-d)). In $CDCl_3$, the two doublets of the aromatic

protons are found in the range 5.87–5.93 ppm and converge into a *pseudo*-quartet, with $\Delta\nu_{AB}$ = 8 Hz. In DMSO, the two doublets are further apart from each other ($\Delta\nu_{AB}$= 25 Hz) and shifted downfield by about 0.3 ppm in comparison to the corresponding signals in $CDCl_3$, which suggests that DMSO acts here as hydrogen bond acceptor. Such intermolecular interactions might be of importance for interaction of the complex with the biological target(s).

2.2 ^{1}H NMR spectrum of 3

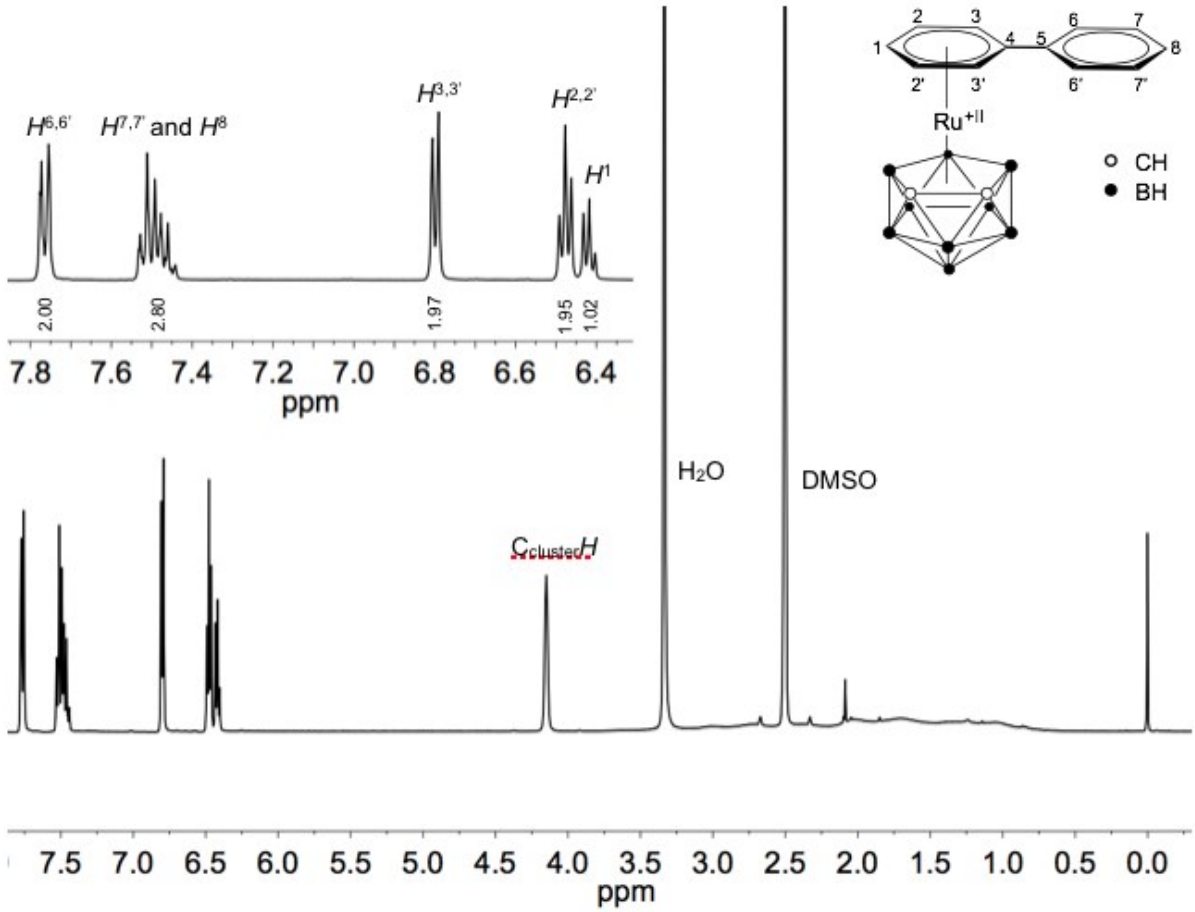

Figure S2. ^{1}H NMR spectrum of **3** in DMSO-d_6. Inset shows expansion of the aromatic region. Assignment of aromatic protons of **3** is shown.

2.3 Expansion of ^{1}H NMR spectra of biphenyl, Ru3 and 3

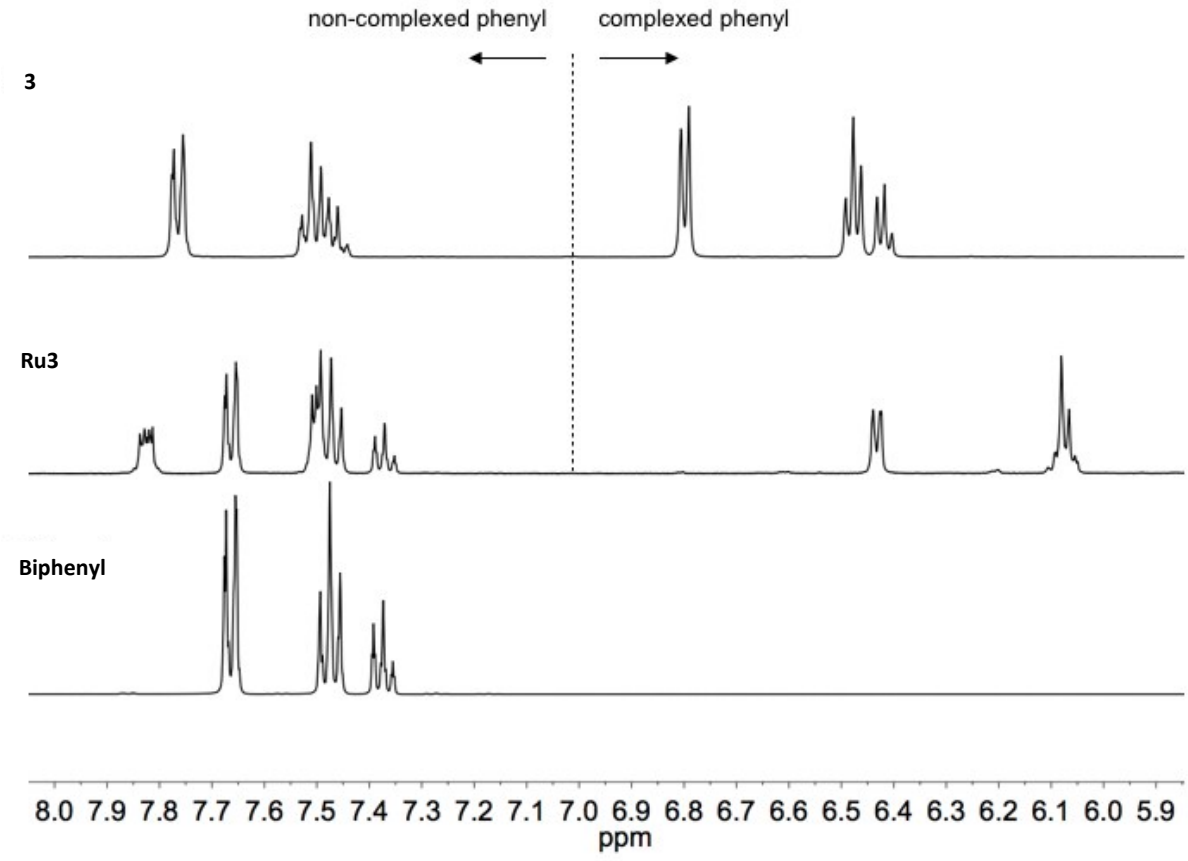

Figure S3. Expansion of the aromatic region of the ^{1}H NMR spectra of **3**, **Ru3** and biphenyl. Signals corresponding to complexed and non-complexed arene for **3** and **Ru3** are shown.

2.4 ^{1}H and $^{11}B\{^{1}H\}$ NMR spectra of 4

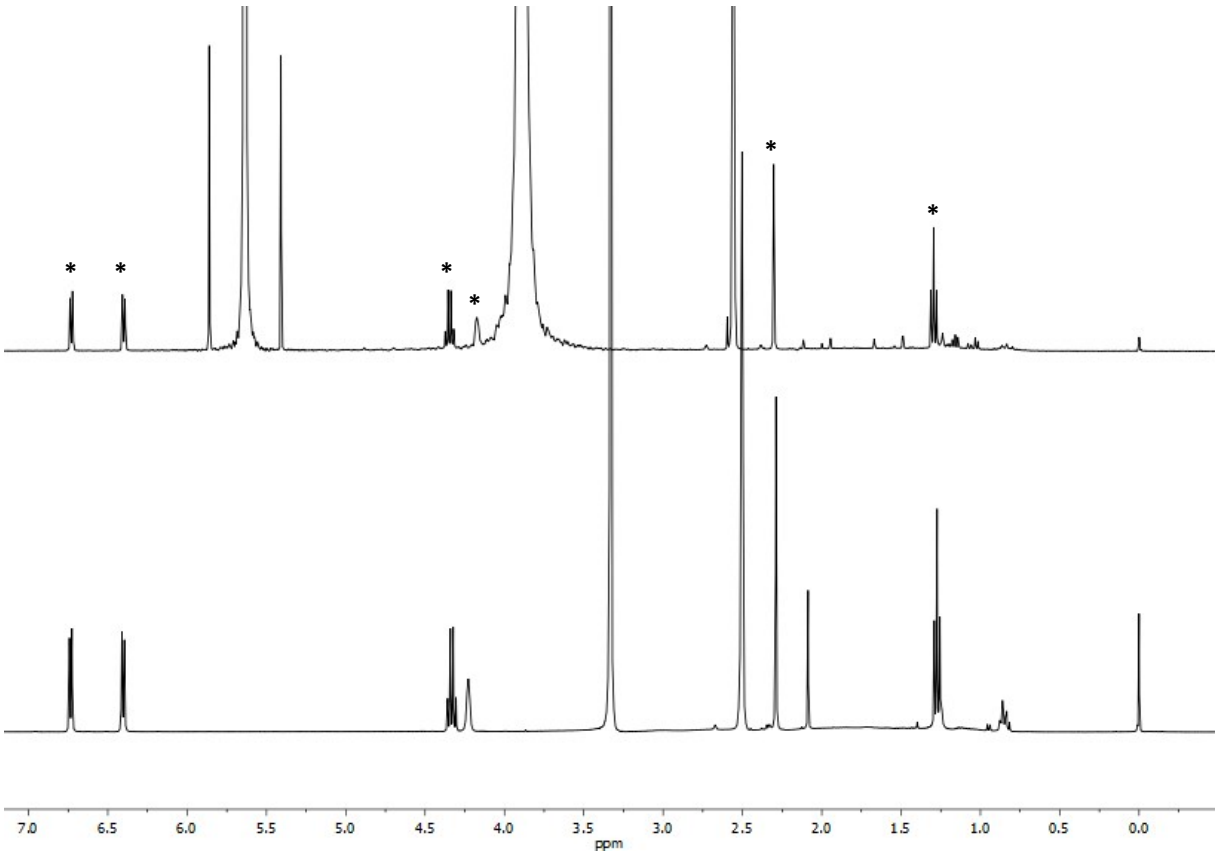

Figure S4. ^{1}H NMR spectra in DMSO-d_6 of freshly dissolved **4** (bottom) and of **4** after stirring for 72 h at 37 °C in DMSO/saline solution (top). Signals belonging to **4** are marked with ***** in the upper spectrum. No changes in the proton signals were found.

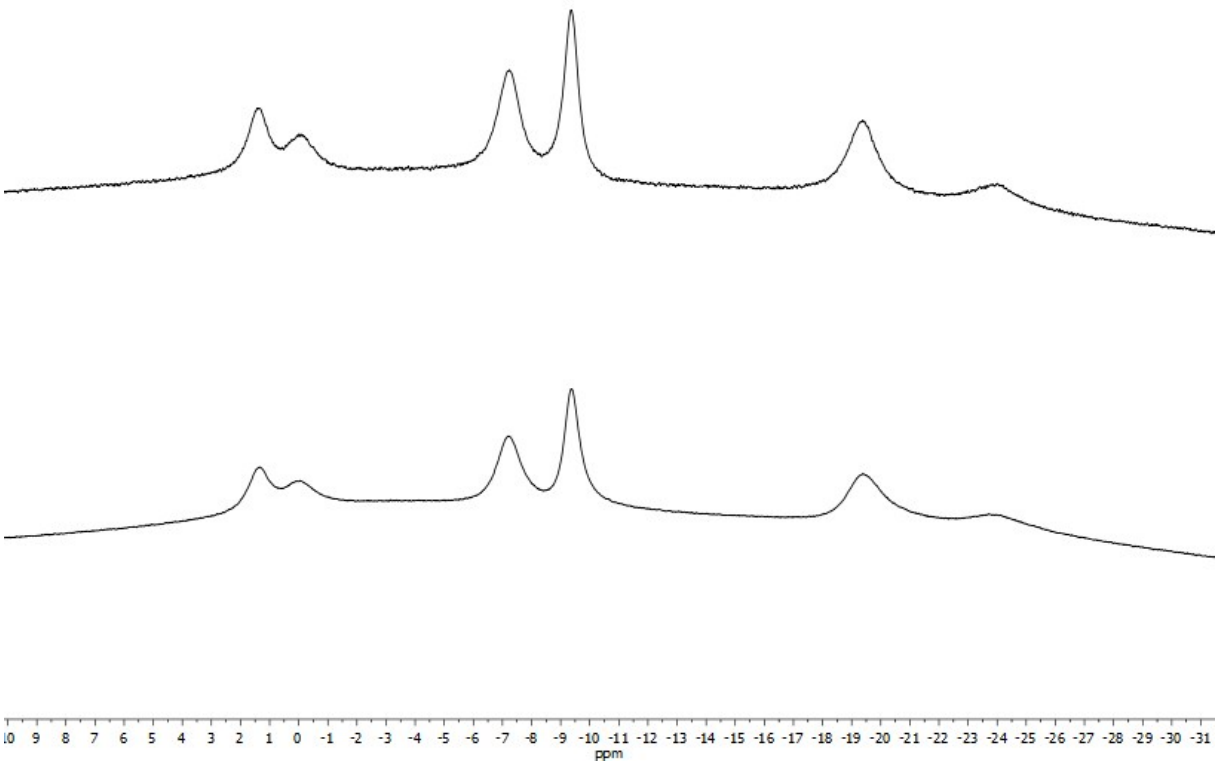

Figure S5. $^{11}B\{^{1}H\}$ NMR spectra in DMSO-d_6 of freshly dissolved **4** (bottom) and of **4** after stirring for 72 h at 37 °C in DMSO/saline solution (top). No changes in the boron signals were found.

3 Crystallographic Data

3.1 Data collection and refinement data

Table S1. Data collection and refinement data for **2**, **3** and **4**.

		2	**3**	**4**
	Empirical formula	$C_{12}H_{25}B_9Ru$	$C_{14}H_{21}B_9Ru$	$C_{12}H_{23}B_9O_2Ru$
	Molecular weight	367.68 g mol^{-1}	387.67 g mol^{-1}	397.66 g mol^{-1}
Data collection				
	Reflections collected	47341	29371	36692
	Independent reflections	11241 (R_{int} = 0.0364)	5696 (R_{int} = 0.0425)	8455 (R_{int} = 0.0330)
	Θ_{max}	32.475°	32.498°	37.433°
	Completeness (%)	100.0	100.0	100.0
	Crystal system	Monoclinic	Monoclinic	Monoclinic
	Unit cell	*a* = 20.0453(4) Å *b* = 8.0704(1) Å *c* = 21.0222(4) Å β = 100.727(2)°	*a* = 11.3260(2) Å *b* = 10.9993(2) Å *c* = 13.5471(2) Å β = 97.546(2)°	*a* = 8.3684(1) Å *b* = 12.5136(1) Å *c* = 16.4655(2) Å β = 103.914(1)°
	Volume	3341.4(1) Å^3	1673.06(5) Å^3	1673.65(3) Å^3
	Space group	$P2_1/n$	$P2_1/c$	$P2_1/n$
	Z	8	4	4
	ρ_{calc}	1.462 Mg m^{-3}	1.539 Mg m^{-3}	1.578 Mg m^{-3}
	μ(Mo-K_α)	0.923 mm^{-1}	0.926 mm^{-1}	0.936 mm^{-1}
Refinement				
	Data/parameters/restraints	11241/534/26	5696/301/0	8455/309/6
	R (I > 2σI)	0.0391	0.0289	0.0272
	R_w (I > 2σI)	0.0723	0.0575	0.0590
	R (all data)	0.0519	0.0379	0.0350
	R_w (all data)	0.0755	0.0606	0.0623
	Max. / Min. residual electron density	0.834 / –0.663 e·Å^{-3}	0.870 / –0.665 e·Å^{-3}	1.378 / –0.689 e·Å^{-3}
	Goodness-of-fit on F^2	1.168	1.057	1.081

3.2 Molecular structure of compound 2, 3 and 4

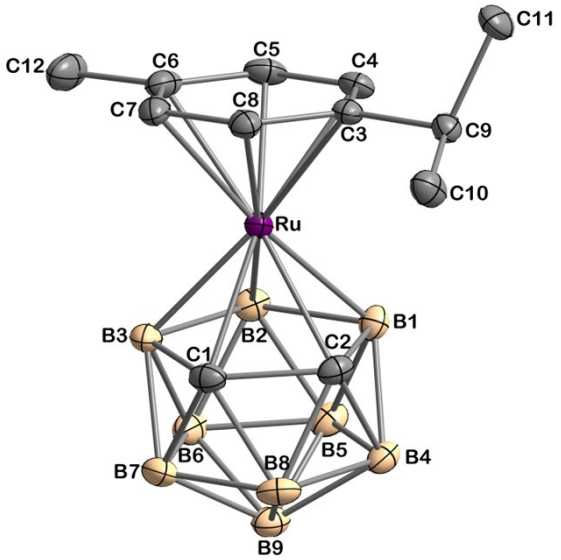

Figure S6. Molecular structure of **2**, showing atom labelling. Only one of the two symmetry-independent molecules is shown. Thermal ellipsoids at 50% probability. Hydrogen atoms are omitted for clarity.

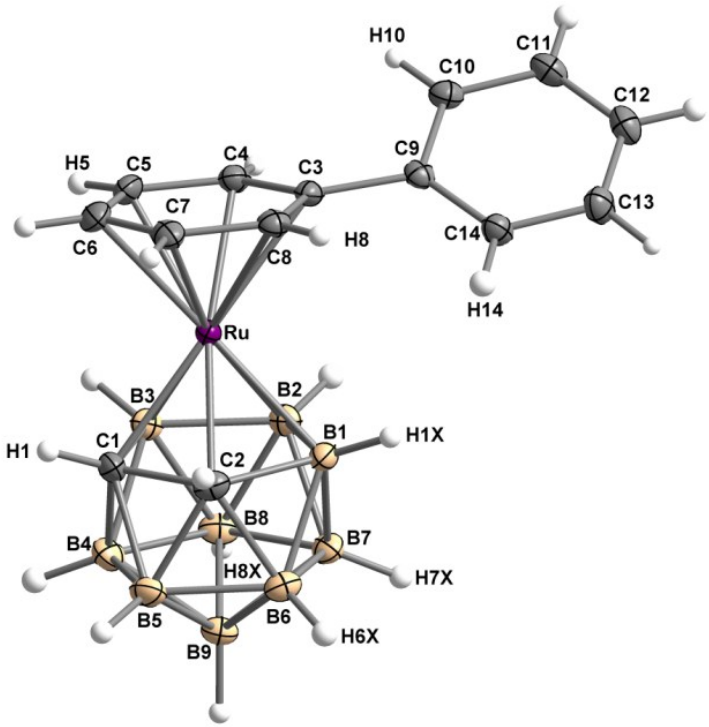

Figure S7. Molecular structure of **3**, showing atom labelling. Thermal ellipsoids at 50% probability.

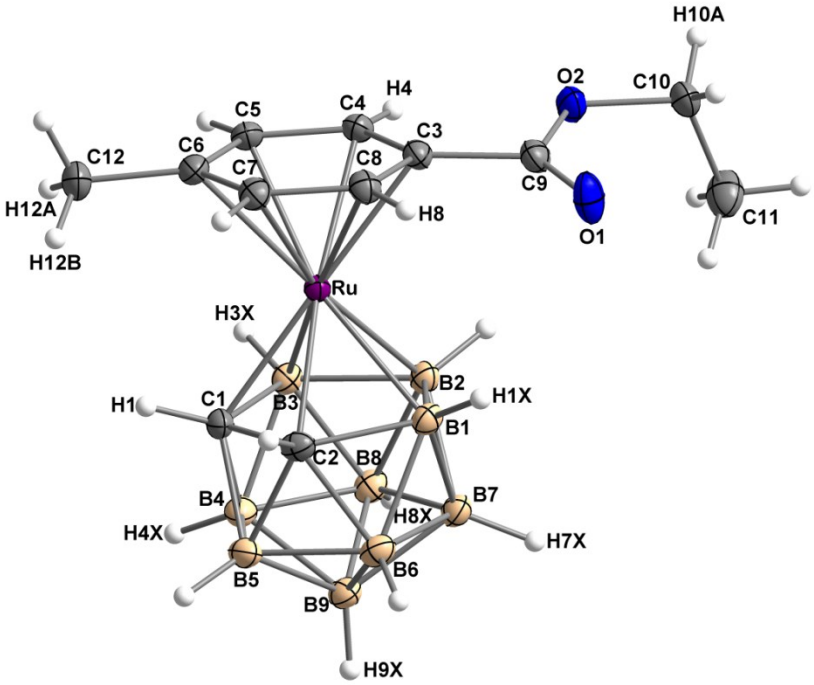

Figure S8. Molecular structure of **4**, showing atom labelling. Thermal ellipsoids at 50% probability.

3.3 Selected distances and angles for compound 3

Table S2(a,b). Selected distances (Å) and angles (°) for **3**.

a)

Distances	Values (Å)
H(5)–Ctd3[a]	2.68(2)
H(8X)–H(8)	2.40(3)
H(7X)–H(10)	2.35(3)
H(1)–H(6X)	2.36(3)

[a] Ctd3 = centroid of the non-coordinated arene (C(9)–C(10)–C(11)–C(12)–C(13)–C(14)).

b)

Angles	Values (°)
C(5)–H(5)–Ctd3	151.8(2)
C(8)–H(8)–H(8X)	118.0(2)

B(8)–H(8X)–H(8)	119.1(2)
B(7)–H(7X)–H(10)	129.3(2)
H(7X)–H(10)–C(10)	166.1(2)
C(1)–H(1)–H(6X)	154.5(2)
H(1)–H(6X)–B(6)	106.6(2)
C(14)–H(14)–H(1X)	125.1(2)
B(1)–H(1X)–H(14)	136.7(2)

3.4 Compound 4: crystal packing, selected distances and angles

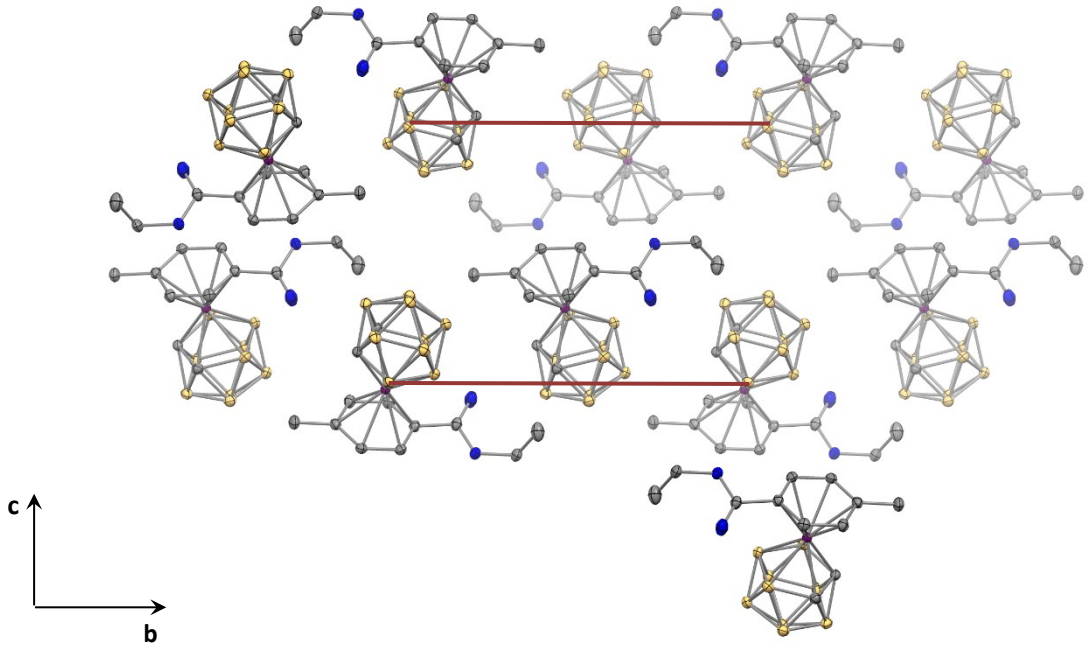

Figure S9. Crystal packing of **4** viewed along the *a* axis. Thermal ellipsoids at 50% probability. 2_1 axis along *b* is shown in brown. Hydrogen atoms are omitted for clarity.

Table S3(a,b). Selected distances (Å) and angles (°) for **4**.

a)

Distances	Values (Å)
Ctd1–O(2)[a]	3.543(1)
H(12B)–H(1X)	2.43(3)
H(10A)–H(7X)	2.36(3)
H(3X)–H(4)	2.30(3)
H(12A)–H(9X)	2.45(3)
H(8X)–H(8)	2.45(3)
O(1)–H(2)	2.56(2)

[a]According to Jain *et al.* (2009),[1] non-covalent interactions between a π system and a lone pair of electrons (lp) of an oxygen atom (lp···π) have been identified for oxygen atoms of water molecules. Typical distances π(centroid)–O are ≤ 3.5 Å.

b)

Angles	Values (°)
C(12)–H(12B)–H(1X)	134(1)
B(1)–H(1X)–H(12B)	154(1)
C(10)–H(10A)–H(7X)	167(2)
B(7)–H(7X)–H(10A)	120(1)
C(4)–H(4)–H(3X)	147(1)
B(3)–H(3X)–H(4)	119(1)
C(12)–H(12A)–H(9X)	128(2)
B(9)–H(9X)–H(12A)	130(1)
O(1)–H(2)–C(2)	138(1)
O(2)–Ctd1–C(arene)*	90.3(5)

* average value. The O–centroid–C_{arene} reported by Jain *et al.* is in the range of 80 to 110°.[1]

4 Frontier Molecular Orbitals

4.1 Frontier molecular orbitals of 2 and 2-Cp

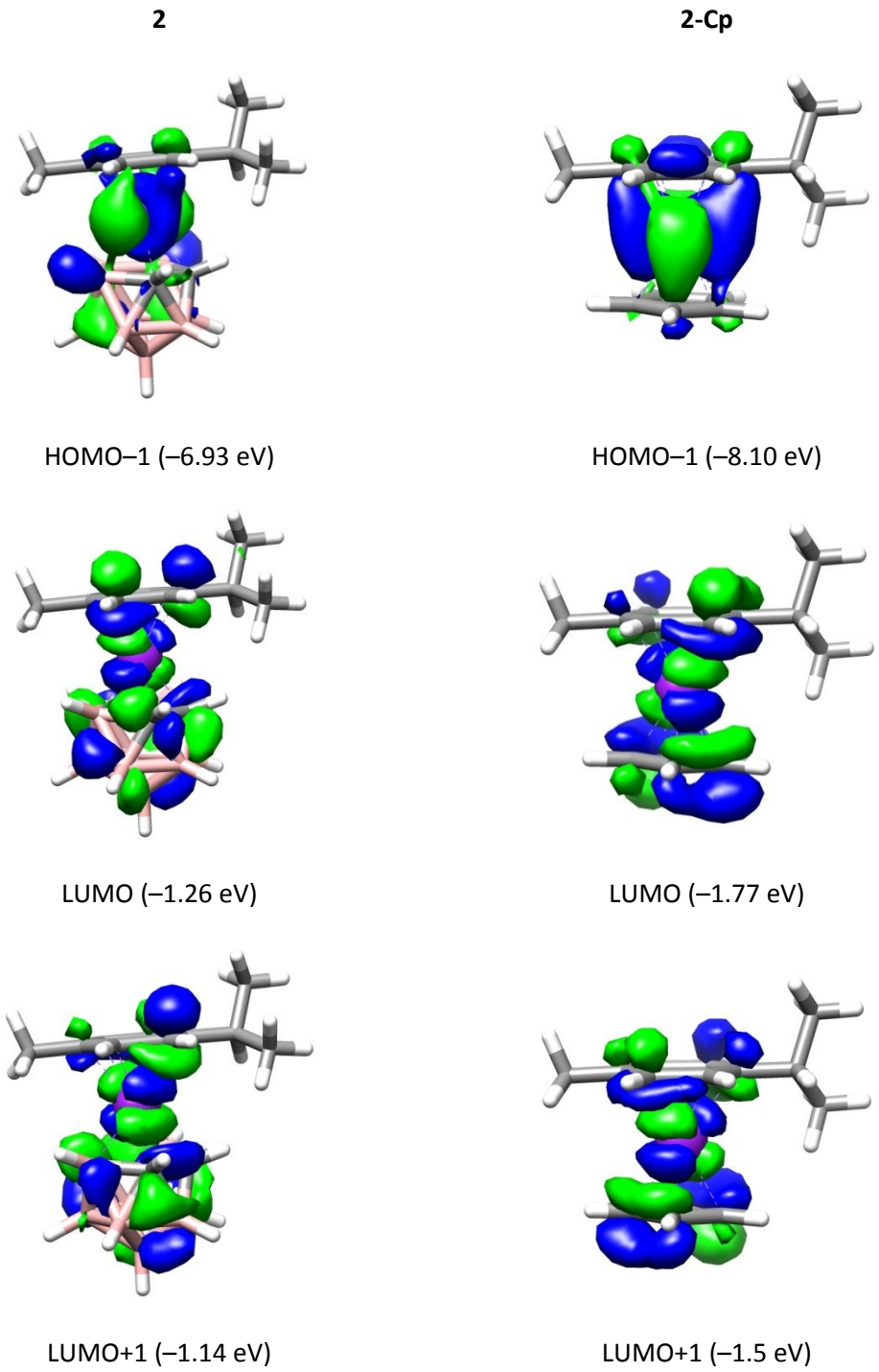

Figure S10. Frontier molecular orbitals of **2** and **2-Cp**.

4.2 Frontier molecular orbitals of 3 and 3-Cp

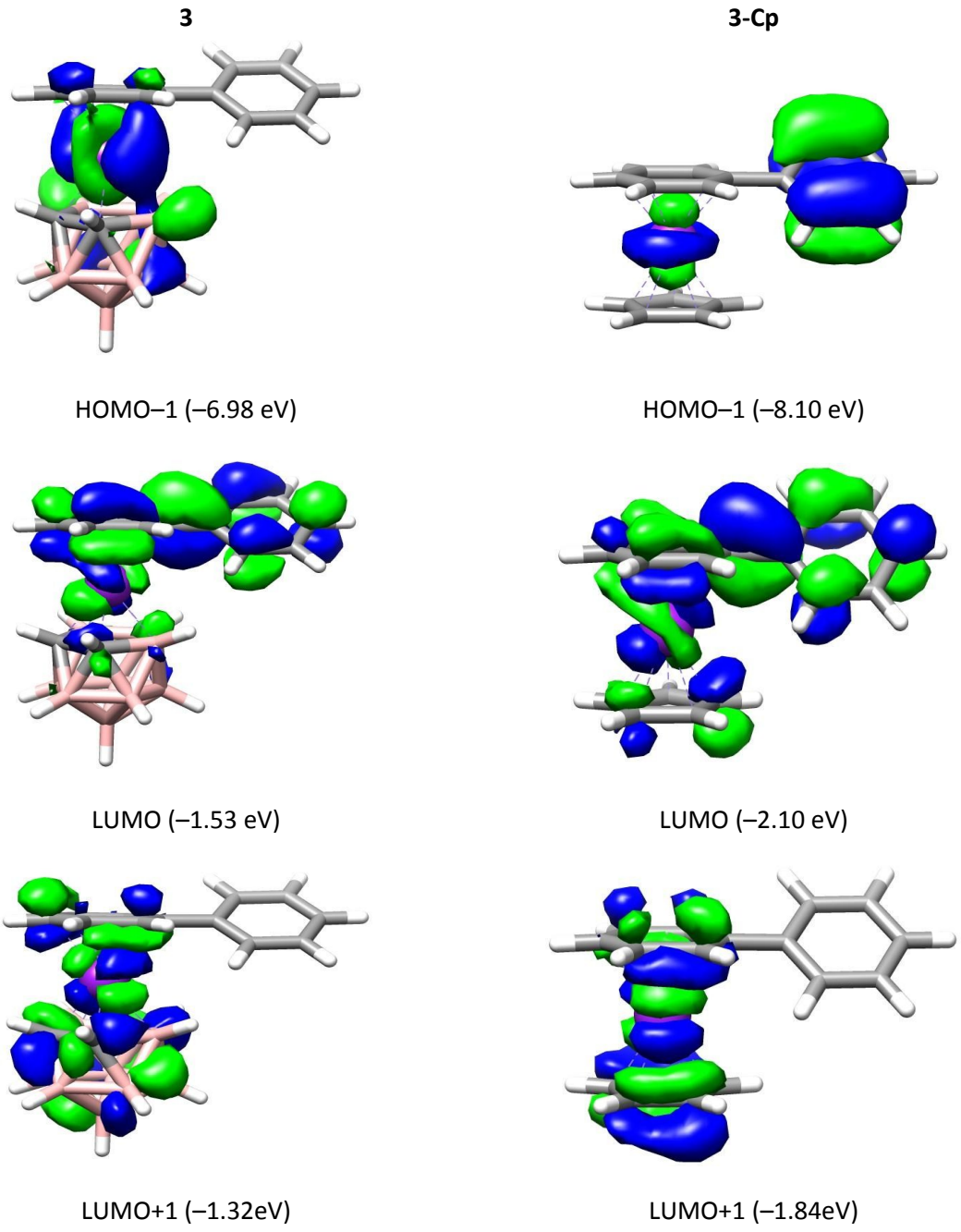

Figure S11. Frontier molecular orbitals of **3** and **3-Cp**.

4.3 Frontier molecular orbitals of 4 and 4-Cp

4 **4-Cp**

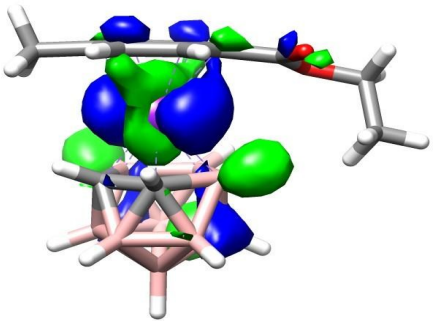

HOMO–1 (–7.11 eV)

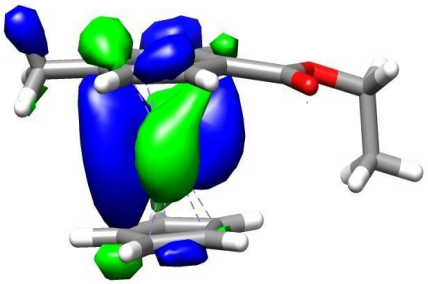

HOMO–1 (–8.37eV)

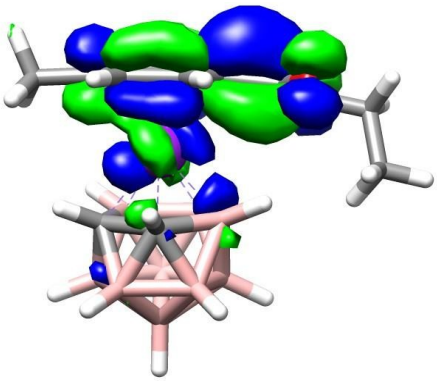

LUMO (–1.72 eV)

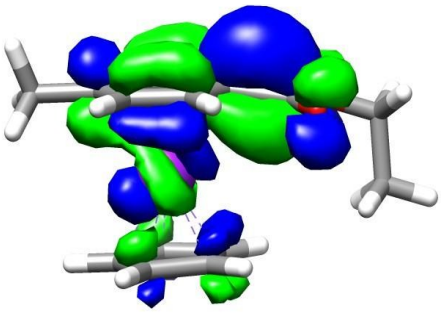

LUMO (–2.47 eV)

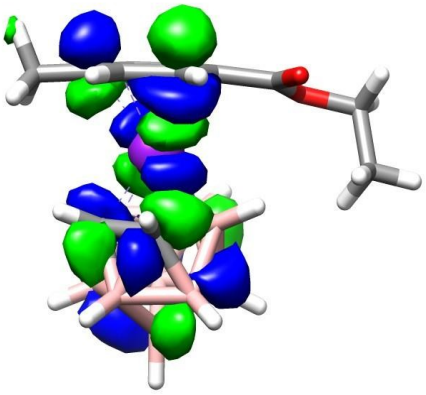

LUMO–1 (–1.42 eV)

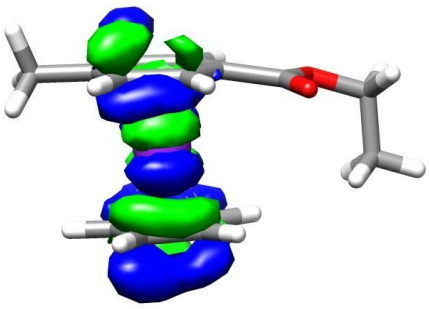

LUMO–1 (–2.00 eV)

Figure S12. Frontier molecular orbitals of **4** and **4-Cp**.

5 Cell viability curves

5.1 Cell viability curves for 2, 3, 4 and cisplatin

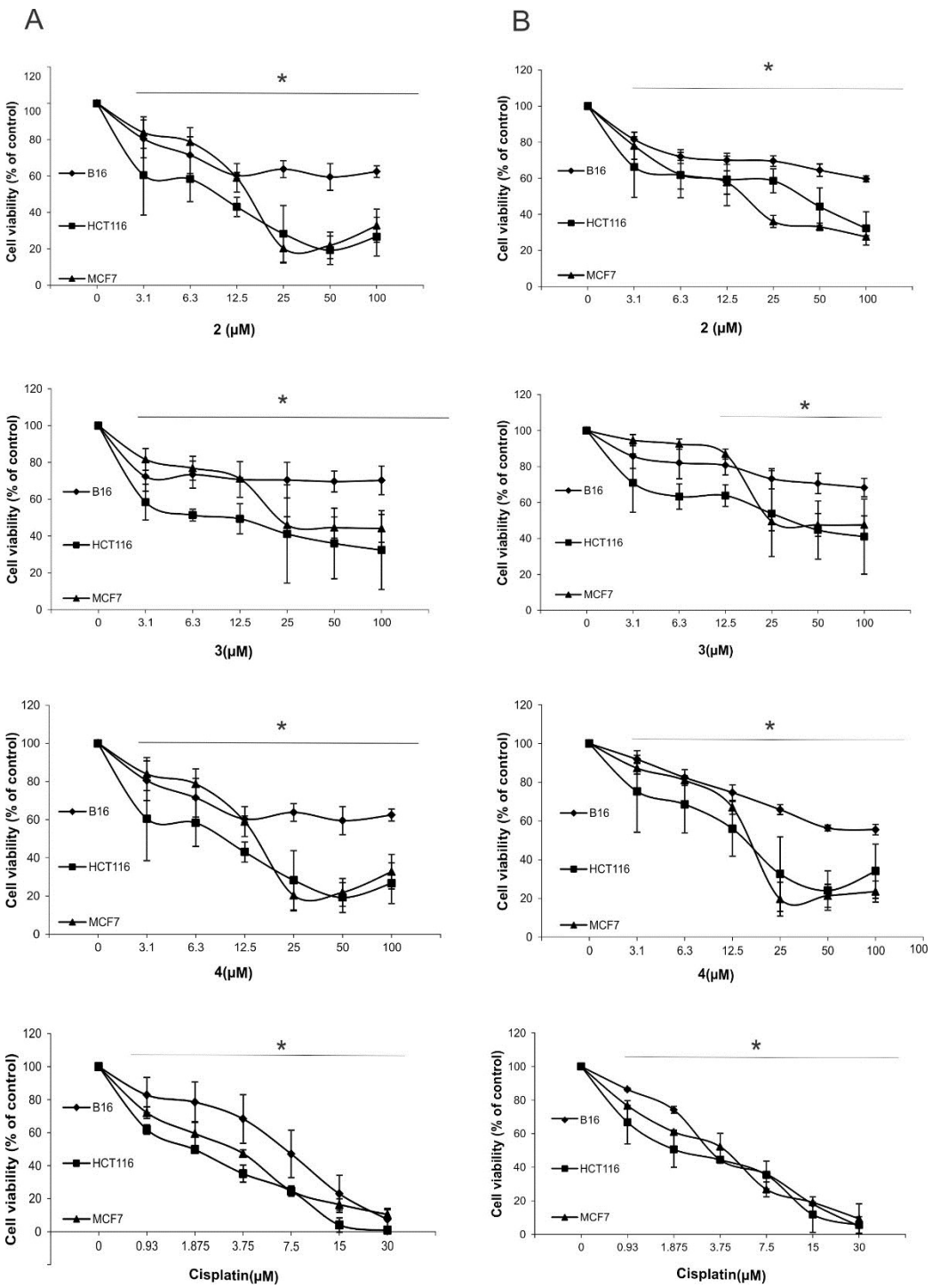

Figure S13. Complexes 2-4 inhibited the growth of tumour cell lines. B16, HCT116 and MCF7 cells were incubated with **2**, **3**, **4** and cisplatin for 72 h and thereafter viability was analysed by MTT (column A, left) and CV (column B, right). Results calculated from three repeated experiments are shown. Statistically significant values ($p<0.05$) are marked with *.

5.2 Incubation of macrophages, MLEC cells and MRC-5 cells with 4

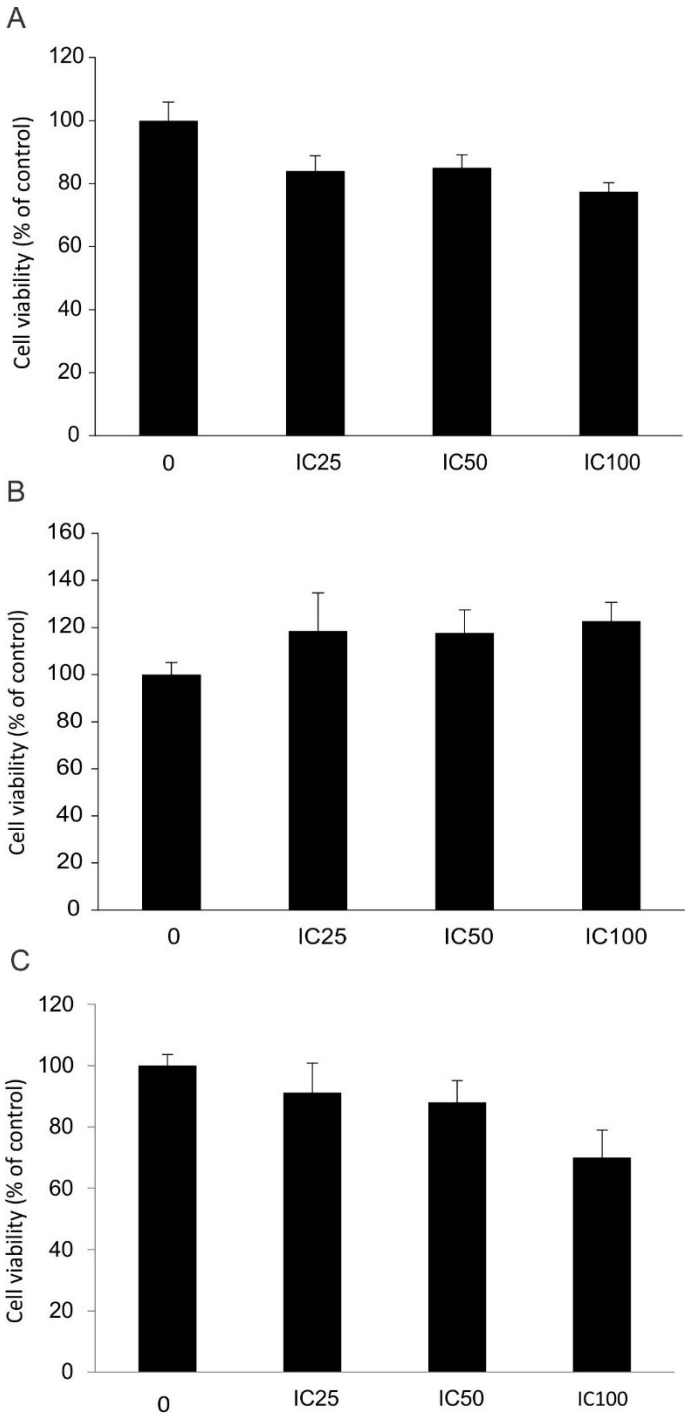

Figure S14. Complex 4 did not affect the viability of normal cells. Peritoneal macrophages (**A**), MLEC (**B**) and MRC-5 (C) cell line were incubated with IC_{25}, IC_{50} and IC_{100} doses of **4** (values obtained from tumour cell lines). Cell viability was analysed by MTT assay. Results from representative of three repeated experiments with the same experimental conditions are presented. 0 stands for control (untreated cells).

6 UV-vis spectra of PBS/DMSO and BSA in PBS with complex 3

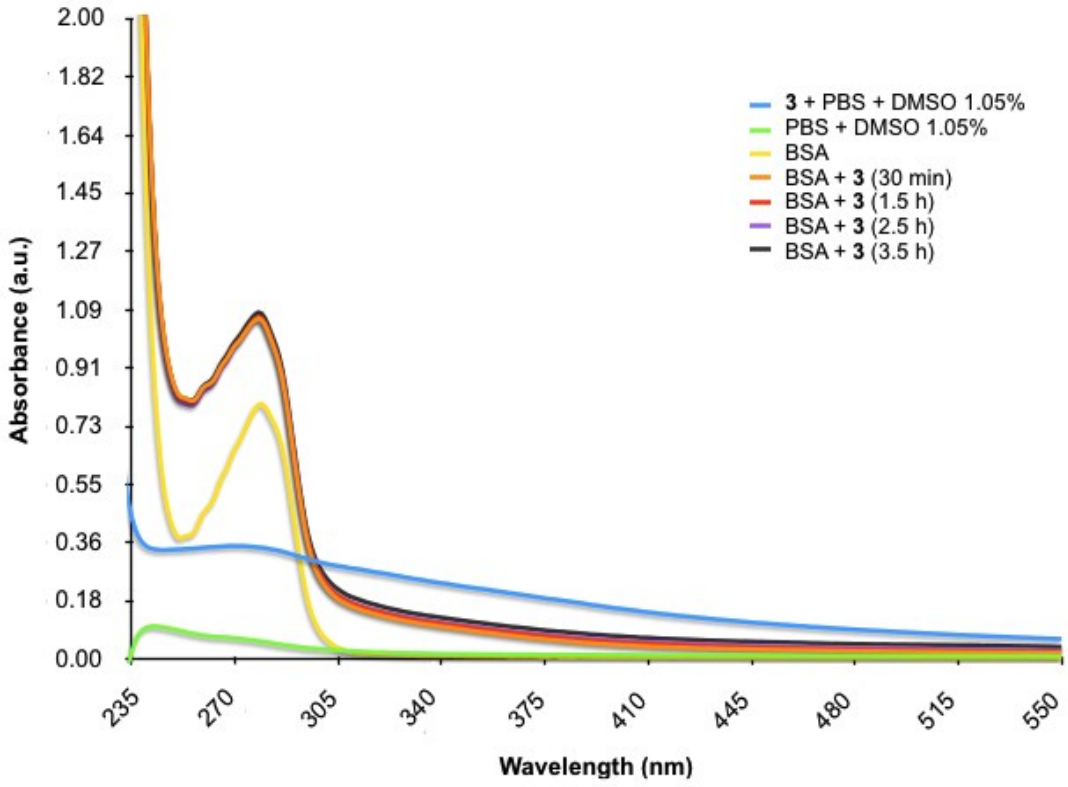

Figure S15. Effect of **3** on the UV-vis absorption spectra of PBS/DMSO and BSA (in PBS) solutions at room temperature (pH = 7.4). [BSA] = 2.0 x 10–5 M; [**3**] = 20 µM. Absorption spectra of PBS/DMSO (green curve) and BSA (in PBS; yellow curve) without complex **3** are also shown. Increase of BSA absorption at 278 nm upon incubation with **3** indicates formation of a protein-drug complex in solution. No variation of BSA+**3** absorption intensity at 278 nm over time, in the time-scale of the experiments, was found.

7 List of Abbreviations

ANN(V)	Annexin V-FITC
B16	mouse melanoma
BNCT	boron neutron capture therapy
BSA	bovine serum albumin
br (NMR)	broad
Cb^{2-}	dicarbollide, $C_2B_9H_{11}^{2-}$
CFSE	carboxyfluorescein succinimidyl ester
Cp	cyclopentadienyl

Cp*	pentamethylcyclopentadienyl
CV	crystal violet
p-cymene	1-methyl-4-isopropyl-benzene
d (NMR)	doublet
DFT	density functional theory
DMSO	dimethylsulfoxide
EDTA	ethylendiamminetetraacetic acid
FA	formic acid
FCS	fetal calf serum
h	hour(s)
hept (NMR)	heptet
HOMO	highest occupied molecular orbital
HTC-116	human colon carcinoma
IC_{50}	half-maximal inhibitory concentration
LUMO	lowest unoccupied molecular orbital
m (IR)	medium
m (NMR)	multiplet
M.p.	melting point
3-MA	3-methyl adenine
MCF-7	human breast carcinoma
Mf	mouse peritoneal macrophages
MRC-5	primary transformed fibroblasts
MLEC	mouse endothelial lung cells
MTT	3-(4,5-dimethylthiazol-2-yl)-2,5-diphenyltetrazolium bromide
PBS	phosphate-buffered saline
Ph	phenyl
PI	propidium iodide

q (NMR)	quartet
RNase	ribonuclease
r.t.	room temperature
s (IR)	strong
s (NMR)	singlet
t (NMR)	triplet
THF	tetrahydrofuran
TLC	thin layer chromatography
w (IR)	weak

8 References

1. A. Jain, V. Ramanathan, R. Sankararamakrishnan, *Protein Sci.,* 2009, **18**, 595.